Critical state-based interpretation of the monotonic behaviour of Hostun sand

Ricardo J. N. Azeiteiro [(1)] [(*)], Paulo A. L. F. Coelho [(2)], David M. G. Taborda [(3)] and José C. D. Grazina [(4)]

[(1)] PhD candidate, Department of Civil Engineering, University of Coimbra, Coimbra, Portugal, ricardoazeiteiro@uc.pt, [(*)] corresponding author
[(2)] Assistant Professor, Department of Civil Engineering, University of Coimbra, Coimbra, Portugal, pac@dec.uc.pt
[(3)] Lecturer, Department of Civil and Environmental Engineering, Imperial College London, London, U.K, d.taborda@imperial.ac.uk
[(4)] Assistant Professor, Department of Civil Engineering, University of Coimbra, Coimbra, Portugal, graza@dec.uc.pt

Abstract

A series of bender element tests and drained and undrained monotonic triaxial compression and extension tests were performed on air-pluviated samples of Hostun sand. Samples were prepared to different initial void ratios, consolidated under various isotropic and anisotropic stress states and sheared using different stress-paths and a wide range of deformations to characterise the sand's stress-strain response. The results suggest that the sand's small-strain behaviour essentially depends on the current void ratio and mean effective stress. Within the medium to large strain range, a state parameter approach in conjunction with the critical state framework can successfully predict the distinctive states of the sand's monotonic response, namely the phase transformation, the peak stress ratio and the critical states. Furthermore, the data is used to examine a stress-dilatancy relationship often incorporated in constitutive models. The characterisation presented herein aims at assisting the efficient calibration of numerical models and provides insight into this sand's behaviour, thus supporting the interpretation of results of physical modelling involving this sand. This paper highlights the importance of characterising sand's behaviour over the full strain range and shows that accurate predictions of the critical state and small-strain stiffness are crucial to assess other aspects of the sand's behaviour.

Keywords: bender element tests; triaxial testing; dilatancy; peak strength; critical state; state parameter.

Introduction

In recent years, state parameter approaches (Been and Jefferies 1985) have been increasingly used in conjunction with the Critical State Soil Mechanics (Schofield and Wroth 1968) framework to establish constitutive models capable of describing the behaviour of sand under general loading conditions (e.g. Manzari and Dafalias 1997; Ling and Yang 2006), as well as for the interpretation of site investigation data in sands (e.g. Been *et al.* 1987; Konrad 1998). Indeed, the state parameter concept appears to be an effective form of predicting the occurrence of relevant features of the response of sand, such as phase transformation and strain softening after a peak stress ratio state, for a wide range of densities and stress states (e.g. Been and Jefferies 1985; Ishihara 1993; Jefferies and Been 2006). Furthermore, it has been suggested that the capabilities of a model to reproduce the behaviour of sand can be improved by considering a state-dependent dilatancy (e.g. Manzari and Dafalias 1997; Gajo and Wood 1999; Li and Dafalias 2000; Yang and Li 2004).

In this paper, the key features of the monotonic response of air-pluviated Hostun sand are assessed by employing a state parameter approach, i.e. by using the difference between the current void ratio and the void ratio at critical state corresponding to the current mean effective stress (Been and Jefferies 1985). For this purpose, results of an extensive laboratory testing program performed on air-pluviated Hostun sand are presented. This includes both bender element (BE) and triaxial testing on samples prepared with different initial densities and consolidated under several isotropic and anisotropic stress states. Results of BE tests are firstly reported and used to characterise the behaviour of the air-pluviated sand at small-strains. Subsequently, results of drained and undrained monotonic triaxial compression (TC) and extension (TE) tests are presented and the behaviour of sand within the medium to large strain range is depicted. In order to use a state parameter approach, focus is firstly given to the prediction of the critical state (CS). Subsequently, the occurrence of both the phase

transformation and the peak stress ratio states are examined as a function of the state parameter and the stress-dilatancy behaviour of Hostun sand is investigated.

The extensive and comprehensive experimental data presented in this paper can be used as reference for the calibration of constitutive relationships, as well as for the characterisation of the ability of such constitutive models to reproduce the distinctive features of the behaviour of sand examined here. Indeed, since the adequate numerical simulation of the behaviour observed in centrifuge models requires the availability of reliable data on the materials used in those experiments, this experimental dataset and its detailed interpretation aims at bridging the gap between centrifuge and numerical modelling. As explained later, this can be particularly valuable for Hostun sand.

Laboratory testing programme

Tested material

All tests in this experimental programme were performed on Hostun RF sand, which is a fine-grained, sub-angular to angular, siliceous sand (Flavigny *et al.* 1990). The sand is uniformly graded between no. 20 (0.850 mm) and no. 200 (0.075 mm) sieves of ASTM series (Fig. 1). The mean particle diameter, D_{50}, and the uniformity coefficient, C_u, are close to 0.33 mm and 1.4, respectively (Table 1). The density of soil particles, G_s, is 2.64 and the minimum and maximum void ratios, e_{min} and e_{max}, determined according to ASTM D4253-00 (2006) and ASTM D4254-00 (2006), are close to 0.66 and 1.00, respectively.

This sand has been extensively studied over the last three decades, particularly at the Grenoble Institute of Technology (INPG), where it has been used as a reference material. Among the several research projects carried out at INPG, the one developed in collaboration with Case Western Reserve University is of particular relevance to the work presented in this paper. Indeed, the experimental data obtained in this research project, where Hostun sand was tested

both in a cubic cell device and a hollow cylinder torsional apparatus, was used to assess the predictive capabilities of several constitutive models (Saada *et al.* 1989). Moreover, it is noteworthy the use of Hostun sand at INPG for the study of strain localisation during shearing (e.g. Desrues *et al.* 1996; Mokni and Desrues 1999), as well as for examining the undrained behaviour of very loose samples, particularly the onset of flow deformation (e.g. Konrad 1993). Further research on the latter topic was carried out at *École Nationale des Travaux Publics de l'État* (ENTPE), where the influence of consolidation characteristics on the unstable behaviour of very loose samples of Hostun sand was assessed (e.g. Doanh *et al.* 1997).

This sand was also used at *École Nationale des Ponts et Chaussées* (ENPC) for studying the influence of the loading path (e.g. De Gennaro *et al.* 2004) and of the inherent anisotropy created by different methods of sample preparation (e.g. Benahmed 2001) on its behaviour.

Despite the extensive element laboratory testing carried out on this sand, Gajo and Wood (1999) observed that, since previous laboratory testing programmes were focused on particular aspects of soil behaviour, it is not possible to find in the literature a comprehensive set of drained and undrained element laboratory tests on samples of Hostun sand prepared using a single method of sample reconstitution and covering a wide range of initial density and stress conditions to be used in numerical modelling. Therefore, the present laboratory testing programme aims at addressing this gap, providing reliable data to the calibration and validation of constitutive models. Furthermore, the recent use of Hostun sand on centrifuge modelling (e.g. Marques *et al.* 2014; Li and Bolton 2014; Chian *et al.* 2014) highlighted the need for high quality testing to be performed on this material.

Fig. 1 compares the particle size distribution (PSD) of Hostun sand used in the present programme with the gradations used in the aforementioned laboratory studies. It can be observed that only small deviations exist between them. The values found for the minimum

and maximum void ratios are also similar (Table 1), with the small differences between them resulting from the application of different standards.

Typical PSD of other reference sands presented in the literature are also depicted in Fig. 1, with their physical properties being summarised in Table 1. Ottawa sand (Murthy *et al.* 2007) has a similar PSD to that exhibited by Hostun sand, though completely different particle shape, while the opposite is true for Leigthon Buzzard (Been *et al.* 1991) and Toyoura (Verdugo and Ishihara 1996) sands.

Table 1. Physical properties of Hostun, Leighton Buzzard, Ottawa and Toyoura sands

Sand	Hostun RF				Toyoura	Leighton Buzzard	Ottawa
Institution	UC [(1)]	INPG [(2)]	ENTPE [(3)]	ENPC [(4)]	–	–	–
D_{50} (mm)	0.33	0.32-0.35	0.38	0.33-0.38	0.17	0.12	0.39
C_U ( )	1.4	1.7-1.9	1.9	1.6-1.9	1.7	1.5	1.4
Particle shape	sub-angular to angular				sub-angular to angular	sub-angular to angular	rounded
G_s ( )	2.64	2.65	2.65	2.65	2.65	2.65	[(5)]
e_{min} ( )	0.66 [(6)]	0.62	0.62-0.65	0.66	0.60	0.66	0.48
e_{max} ( )	1.00 [(7)]	0.96	0.96-1.04	1.00	0.98	1.01	0.78
Reference	–	[(8)]	[(8)]	[(8)]	Verdugo and Ishihara (1996)	Been *et al.* (1991)	Murthy *et al.* (2007)

Note: [(1)] University of Coimbra (UC); [(2)] Grenoble Institute of Technology (INPG); [(3)] *École Nationale des Travaux Publics de l'État* (ENTPE); [(4)] *École Nationale des Ponts et Chaussées* (ENPC); [(5)] This information is not provided in the reference; [(6)] ASTM D4253-00 (2006); [(7)] ASTM D4254-00 (2006); [(8)] References are mentioned in the text.

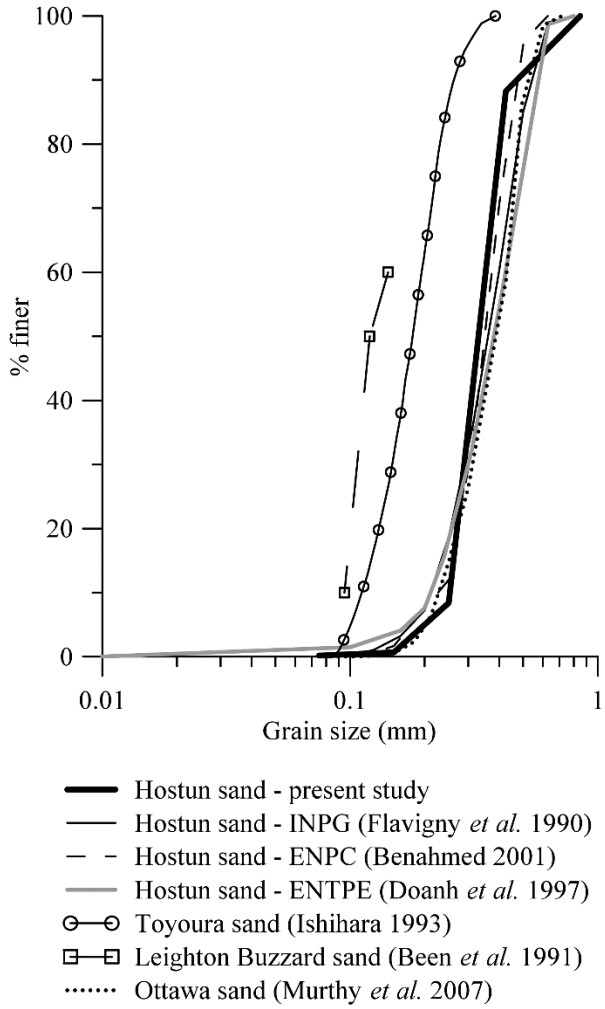


Fig. 1. Particle size distribution curves of Hostun sand, Leighton Buzzard sand, Ottawa sand and Toyoura sand

Laboratory test apparatus and procedures

Triaxial tests

Conventional monotonic compression tests (i.e. with increasing mean stress) were carried out in a triaxial system using 100mm diameter samples with height/diameter ratio close to 2. For monotonic compression tests with decreasing mean stress, as well as for monotonic extension tests, a fully computer-controlled hydraulic triaxial apparatus of the Bishop and Wesley (1975) type, designed for 38 mm diameter specimens, was used. The stress path, in terms of total stresses, followed in each type of test is shown in Fig. 2. A Constant Rate of Strain Pump (CRSP) was used to control the ram pressure, allowing for strain test control. Standard

instrumentation was used: cell and pore water pressure transducers, a submersible load cell, an externally mounted LVDT to measure the axial displacement and a volume gauge to measure changes in sample volume. Further details on these apparatuses can be found in Pedro (2013).

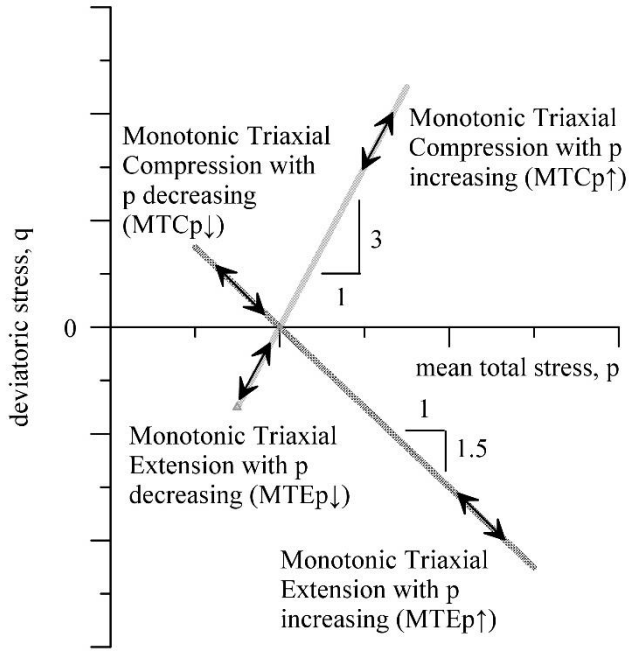


Fig. 2. Schematic representation of the total stress path followed in each type of triaxial test performed

Air-pluviation of dry sand was used to prepare all samples. This technique is known for producing homogeneous samples in clean uniform sands and for its repeatability, which ensures that results can be compared (Coelho 2007). Moreover, since one of the main objectives of the present experimental study was to produce reliable data to be used in the calibration of constitutive models and, subsequently, in the numerical simulation of centrifuge experiments, the frequent application of this technique in centrifuge modelling (Coelho 2007) was considered a major advantage for its selection.

Different initial relative densities were obtained by varying the rate and height of pouring. For loose and moderately loose sand, the rate of pouring was controlled by the size and number of openings of a miniature container. For dense sand, the multiple sieving pluviation technique (Miura and Toki 1982) was employed. Both techniques were methodically tested to ensure

homogeneity and reproducibility. The density of the produced samples was confirmed from mass and volume measurements after preparation. A small suction of about 10 kPa was used to sustain the sample after dismounting the mould used during sand pouring. This value was deemed to be sufficiently low to avoid undesired variations of the void ratio.

All samples were saturated by flowing de-aired water through the sample. A small differential pressure between the top and base of the sample of about 5 kPa was used in order to minimise sample disturbance. A Skempton's B-value above 0.98 was measured in all tests. The back-pressures used during the saturation stage were kept during the consolidation stage to ensure that sample's saturation was preserved.

A first series of drained and undrained tests were performed on samples isotropically consolidated to 25, 50, 80, 135, 200 and 500 kPa (Table 2). Additionally, four drained tests were conducted on anisotropically consolidated samples, in order to compare the responses of samples with similar initial density but subjected to different initial stress conditions.

All tests were performed with a constant axial strain increment of about 6 %/h, which was slow enough to allow for pore pressure changes to equalise throughout the sample. Tests were stopped when the piston reached its maximum displacement, pore water pressure dropped sufficiently for cavitation to occur or a visible shear band developed in the sample.

Bender element tests

In order to evaluate the small strain shear modulus of Hostun sand, BE of the type developed by Dyvik and Madshus (1985) were installed in the Bishop and Wesley's triaxial cell. The transmitter and receiver elements were mounted into the top and base platens of the cell, respectively, protruding about 4.0 mm in length into the sample. A function generator was used to generate the input signal, which was sent both to the transmitter BE and to a digital storage oscilloscope. The vertically propagated wave with horizontal polarisation was then detected by the receiver element, which was also connected to the oscilloscope. Thus, the input and output

signals were displayed simultaneously by the oscilloscope and then transferred to a computer for interpretation. Further information on the BE used in the present study can be found in Pedro (2013), while a detailed description of a similar BE set-up is presented by Alvarado and Coop (2011).

Moderately loose and dense specimens of Hostun sand were prepared using the same procedures described above for triaxial tests and, after complete saturation ($B \approx 0.99$), the samples were gradually consolidated (isotropically) to 25, 55, 80, 110, 135, 165, 200, 300, 400 and 500 kPa. For each stress level, single sine pulses with a peak-to-peak amplitude of 20 V and varying frequencies (from 1 to 10 kHz) were transmitted to the probes, the responses being recorded. A first unloading, a reloading and a second unloading phase were then applied, with BE tests being conducted during each of these stages at isotropic effective stresses of 25, 80, 135, 200, 300, 400 and 500 kPa.

Testing programme

Overall, 34 tests were conducted, with the respective initial conditions and results being summarised in Table 2. As shown, the dataset includes 2 drained isotropic compression tests during which BE tests were performed, 14 drained and 9 undrained monotonic TC tests, as well as 5 drained and 4 undrained monotonic TE tests.

Table 2. Summary of the initial conditions and results of the triaxial tests performed

Test ID †	e_0 ‡ ( )	p'_0 (kPa)	ψ_0 ( )	$e_{end\ test}$ ( )	$p'_{end\ test}$ (kPa)	$q_{end\ test}$ (kPa)	p'_{PTS} § (kPa)	q_{PTS} § (kPa)	η_{PTS} § ( )	ψ_{PTS} § ( )	p'_{PSRS} ‖ (kPa)	q_{PSRS} ‖ (kPa)	η_{PSRS} ‖ ( )	ψ_{PSRS} ‖ ( )
ICDIC 0.794/25	0.794	25.0	-0.142	–	–	–	–	–	–	–	–	–	–	–
ICDIC 0.659/25	0.659	25.0	-0.277	–	–	–	–	–	–	–	–	–	–	–
ICDMTCp↑ 0.875/50	0.875	50.0	-0.071	0.902	102.3	145.9	84.6	105.3	1.244	-0.070	102.9	149.2	1.447	-0.040
ICDMTCp↑ 0.885/80	0.885	80.0	-0.050	0.918	154.2	210.0	138.9	176.9	1.273	-0.049	162.8	237.6	1.458	-0.023
ICDMTCp↑ 0.846/200	0.846	200.0	-0.064	0.881	360.3	473.2	336.4	414.0	1.231	-0.061	379.5	533.1	1.404	-0.035
ICDMTCp↑ 0.835/500	0.835	500.0	-0.040	0.842	871.2	1109.6	867.7	1109.2	1.278	-0.043	927.8	1284.0	1.383	-0.027
ICDMTCp↑ 0.829/25	0.829	25.0	-0.129	0.909	56.1	79.0	40.3	47.6	1.181	-0.124	57.3	87.7	1.528	-0.084
ICDMTCp↑ 0.798/80	0.798	80.0	-0.138	0.874	162.7	224.1	130.4	152.4	1.169	-0.130	169.3	253.0	1.493	-0.086
ICDMTCp↑ 0.804/135	0.804	135.0	-0.118	0.883	258.0	340.1	218.1	250.6	1.149	-0.108	275.6	407.8	1.479	-0.067
ICDMTCp↑ 0.667/25	0.667	25.0	-0.291	0.774	61.2	97.0	37.9	41.6	1.098	-0.285	67.5	122.8	1.816	-0.227
ICDMTCp↑ 0.725/80	0.725	80.0	-0.211	0.847	164.5	220.1	125.4	137.3	1.095	-0.202	183.3	298.2	1.626	-0.158
ICDMTCp↑ 0.728/135	0.728	135.0	-0.195	0.813	265.7	364.2	216.4	245.5	1.135	-0.183	308.1	506.3	1.642	-0.137
ICDMTCp↓ 0.826/80	0.826	80.0	-0.109	0.896	40.7	63.0	49.3	47.8	0.970	-0.129	40.5	63.1	1.557	-0.059
K0CDMTCp↓ 0.797/80	0.797	80.0 (**)	-0.139	0.902	59.8	91.5	–	–	–	–	58.6	93.6	1.597	-0.094
ICDMTCp↓ 0.65/80	0.650	80.0	-0.286	0.864	42.0	54.7	–	–	–	–	34.4	69.7	2.002	-0.255
K0CDMTCp↓ 0.672/80	0.672	80.0 (**)	-0.264	0.881	59.1	90.2	–	–	–	–	51.9	102.4	1.938	-0.213
ICUMTCp↑ 0.876/80	0.876	80.0	-0.059	0.876	535.1	694.1	29.7	36.9	1.241	-0.079	170.4	236.5	1.387	-0.039
ICUMTCp↑ 0.868/80	0.868	80.0	-0.067	0.868	721.8	888.1	28.5	35.6	1.251	-0.087	229.6	312.3	1.360	-0.038
ICUMTCp↑ 0.843/135	0.843	135.0	-0.079	0.843	874.1	1101.6	49.2	56.6	1.151	-0.103	288.9	383.7	1.328	-0.055
ICUMTCp↑ 0.783/25	0.783	25.0	-0.175	0.783	1030.0	1361.4	23.9	17.7	0.742	-0.176	550.3	753.3	1.368	-0.089
ICUMTCp↑ 0.801/80	0.801	80.0	-0.135	0.801	962.7	1246.8	55.5	61.1	1.101	-0.143	494.1	677.4	1.371	-0.075

Test ID [†]	e_0 [‡] ( )	p'_0 (kPa)	ψ_0 ( )	$e_{end\ test}$ ( )	$p'_{end\ test}$ (kPa)	$q_{end\ test}$ (kPa)	p'_{PTS} [§] (kPa)	q_{PTS} [§] (kPa)	η_{PTS} [§] ( )	ψ_{PTS} [§] ( )	p'_{PSRS} [‖] (kPa)	q_{PSRS} [‖] (kPa)	η_{PSRS} [‖] ( )	ψ_{PSRS} [‖] ( )
ICUMTCp↑ 0.815/135	0.815	135.0	-0.108	0.815	1014.5	1340.7	118.6	120.5	1.016	-0.111	785.4	1063.4	1.354	-0.039
ICUMTCp↑ 0.686/25	0.686	25.0	-0.272	0.686	1326.9	2075.0	23.1	24.4	1.056	-0.273	1228.5	1959.7	1.595	-0.142
ICUMTCp↑ 0.751/80	0.751	80.0	-0.185	0.751	1223.4	1789.6	78.8	18.4	0.234	-0.185	1018.1	1582.4	1.554	-0.089
ICUMTCp↑ 0.694/135	0.694	135.0	-0.229	0.694	1306.0	1979.9	121.0	107.3	0.887	-0.232	1305.6	1980.2	1.516	-0.131
ICDMTEp↑ 0.83/80 [(*)]	0.830	80.0	-0.106	0.827	247.7	-250.4	227.7	-223.5	-0.982	-0.095	257.6	-269.1	-1.039	-0.084
K0CDMTEp↑ 0.835/80 [(*)]	0.835	80.0 [(**)]	-0.101	0.826	355.5	-352.0	314.3	-293.1	-0.933	-0.085	369.3	-376.1	-1.002	-0.071
ICDMTEp↑ 0.591/80 [(*)]	0.591	80.0	-0.345	0.643	176.0	-145.6	242.2	-246.1	-1.016	-0.322	407.5	-497.1	-1.210	-0.285
K0CDMTEp↑ 0.602/80 [(*)]	0.602	80.0 [(**)]	-0.334	0.592	505.9	-581.6	372.9	-381.6	-1.023	-0.301	505.8	-581.6	-1.090	-0.283
ICDMTEp↓ 0.793/80 [(*)]	0.793	80.0	-0.139	0.836	57.4	-67.9	60.0	-61.1	-1.019	-0.151	57.0	-69.0	-1.204	-0.131
ICUMTEp↓ 0.79/25 [(*)]	0.790	25.0	-0.167	0.790	300.5	-319.0	20.3	-16.6	-0.819	-0.170	43.9	-49.3	-1.125	-0.158
ICUMTEp↓ 0.839/80 [(*)]	0.839	80.0	-0.097	0.839	316.9	-320.3	49.3	-51.6	-1.047	-0.107	65.5	-72.7	-1.110	-0.102
ICUMTEp↓ 0.658/25 [(*)]	0.658	25.0	-0.299	0.658	239.7	-271.5	22.7	-15.7	-0.692	-0.301	[(***)]	[(***)]	[(***)]	[(***)]
ICUMTEp↓ 0.650/80 [(*)]	0.650	80.0	-0.286	0.650	252.0	-275.9	63.9	-54.3	-0.849	-0.291	[(***)]	[(***)]	[(***)]	[(***)]

Note: [†] The designation identifies: 1) the type of consolidation – IC or K0 for isotropic or anisotropic consolidation, respectively; 2) the type of drainage – D or U for drained or undrained test, respectively; 3) the type of loading – IC for isotropic compression, MTCp↑ for monotonic TC with increasing mean stress, MTCp↓ for monotonic TC with decreasing mean stress, MTEp↓ for monotonic TE with decreasing mean stress and MTEp↑ for monotonic TE with increasing mean stress; 4) the void ratio immediately after consolidation; 5) the mean effective stress immediately after consolidation.

[‡] Post-consolidation values.

[§] PTS: Phase Transformation State.

[‖] PSRS: Peak Stress Ratio State.

[(*)] The adopted sign convention means that the deviatoric stress, q, and, hence, the stress ratio, η, are negative for triaxial extension (TE) tests. However, this is not the case in Fig. 6 and Fig. 7 where the deviatoric stress is always taken as positive in order to enable a direct comparison between the results of triaxial extension and triaxial compression tests.

[(**)] The radial and axial effective stresses at consolidation were 60 and 120 kPa, respectively.

[(***)] When the test was stopped, the stress ratio was still increasing.

Interpretation of element test results

Triaxial tests

Triaxial tests were interpreted in terms of the conventional invariants of stress (the mean effective stress, p', and the deviatoric stress, q) and strains (volumetric strain, ε_v, and deviatoric strain, $\varepsilon_q = 2/3(\varepsilon_a - \varepsilon_r)$). The change in the cross-sectional area of the specimen during both triaxial compression and extension was taken into account by using the right-circular cylinder approach. As previously reported (Klotz and Coop 2002; Been and Jefferies 2004), this area correction is seldom precise, since uniform-strain conditions throughout the sample are rarely observed. This is particularly evident in the case of TE, where strain localisation occurs in the form of specimen necking (e.g. Vaid 2006). Under such conditions, test results seem to be unreliable at large strains, even if more sophisticated area corrections are applied (Yamamuro and Lade 1995). In the present testing programme, sample necking was recurrently observed in all TE tests, irrespective of drainage condition or stress-path direction. Necking was observed to form at axial strains close to 10 %, with the strain accumulation in the necking section intensifying with further strain. Due to the possible unreliability of data obtained after the occurrence of necking, results for axial strains higher than 10 % were disregarded and are not presented in this paper. Nevertheless, it should be highlighted that necking was always observed after the occurrence of phase transformation state and, in the majority of the cases, also after the measurement of the peak stress ratio. Therefore, the inclusion of TE results in the present experimental database is justified by the fact that such tests play an important role in the identification and characterisation of the distinctive states of the monotonic response of Hostun sand, as detailed later.

Corrections regarding the effect of membrane penetration were not taken into account, as they were found to be negligible. Due to the small mean particle diameter of the sand tested and

large diameter of the specimens subjected to TC loading with increasing mean stress, any correction to void ratio at critical state would not exceed 0.002, if the methodology proposed by Baldi and Nova (1984) is employed.

The strains were calculated using the current dimensions of the sample, rather than its initial dimensions, meaning that axial and volumetric strains at a given instant were obtained by integrating all the previously measured strain increments $\delta\varepsilon_a = \delta h/h$ and $\delta\varepsilon_v = \delta V/V$, respectively, where h is the height and V the volume of the sample.

Bender element tests

The small-strain (or maximum) shear modulus, $G_{max,}$ was established based on:

$$G_{max} = \rho V_s^2 = \rho L^2/t^2 \quad (1)$$

where ρ is the density of the sample, V_s is the velocity of the shear wave propagated through the sample, L is the distance between the tips of the BE (Viggiani and Atkinson 1995) and t is the measured travel time.

Although conceptually simple, the determination of G_{max} from BE is not a straightforward task, since distortions in the output signal may mask the arrival of the shear wave (e.g. Sánchez-Salinero *et al.* 1986; Arulnathan *et al.* 1998; Lee and Santamarina 2005). In order to minimise possible misinterpretation of the results, a combined use of time-domain (TD) and frequency-domain (FD) methods was employed, as suggested by Viana da Fonseca *et al.* (2009). Within the TD, the first arrival method was selected, due to its simplicity and widespread use. This method consists on the identification of the instant at which the transmitted excitation first arrives to the receiver, which, in accordance with Viggiani and Atkinson (1995), should be taken as the first significant reversal of polarity of the output signal. The travel time obtained by applying that method was subsequently compared with that resulting from using a FD method. The phase delay method, presented by Alvarado and Coop (2011), was chosen for that purpose. In this method, after the transformation of domain by using a fast Fourier transform

(FFT), the input and output signals are related into a unique transfer function. While the gain factor (i.e. the ratio of the amplitudes of the input to the output signal) can be used to identify the modes of vibration of the system, the phase factor identifies the phase delay between the transmitted and received signals across the frequency spectrum (Alvarado and Coop 2011). Assuming that a BE system is only slightly dispersive and almost unimodal, the phase factor of the transfer function (or of the cross-power spectrum) can be approximated by a straight line, at least over a selected frequency interval, enabling the estimation of the group travel time (e.g. Viggiani and Atkinson 1995; Greening and Nash 2004; Alvarado and Coop 2011). Further details on the principles and application of this method can be found in Viggiani and Atkinson (1995), using the cross-power spectrum, or Alvarado and Coop (2011), using the transfer function.

Behaviour of Hostun sand at small-strains

Results of BE tests are used to examine the behaviour of air-pluviated Hostun sand at small-strains. Fig. 3 presents the time traces for the received signals at the selected stress levels, during the first loading of the ICDIC 0.794/25 test. The presented signals are displayed with reversed polarity (i.e. sine-type traces appear inverted). For clarity of representation, only one time-domain trace is shown for each stress level. Nevertheless, time traces corresponding to input frequencies from 1 to 10 kHz were examined together to identify manually the most likely first arrival of the shear wave at a given confining stress. It appears that the frequencies used (up to 10 kHz) were sufficiently high to reduce significantly near field effects (Sánchez-Salinero *et al.* 1986). Therefore, in general, the first arrival could be identified by the first downward deflection of the received signal, as indicated in the figure. As expected, the higher the stress level, the earlier the shear-wave arrival takes place.

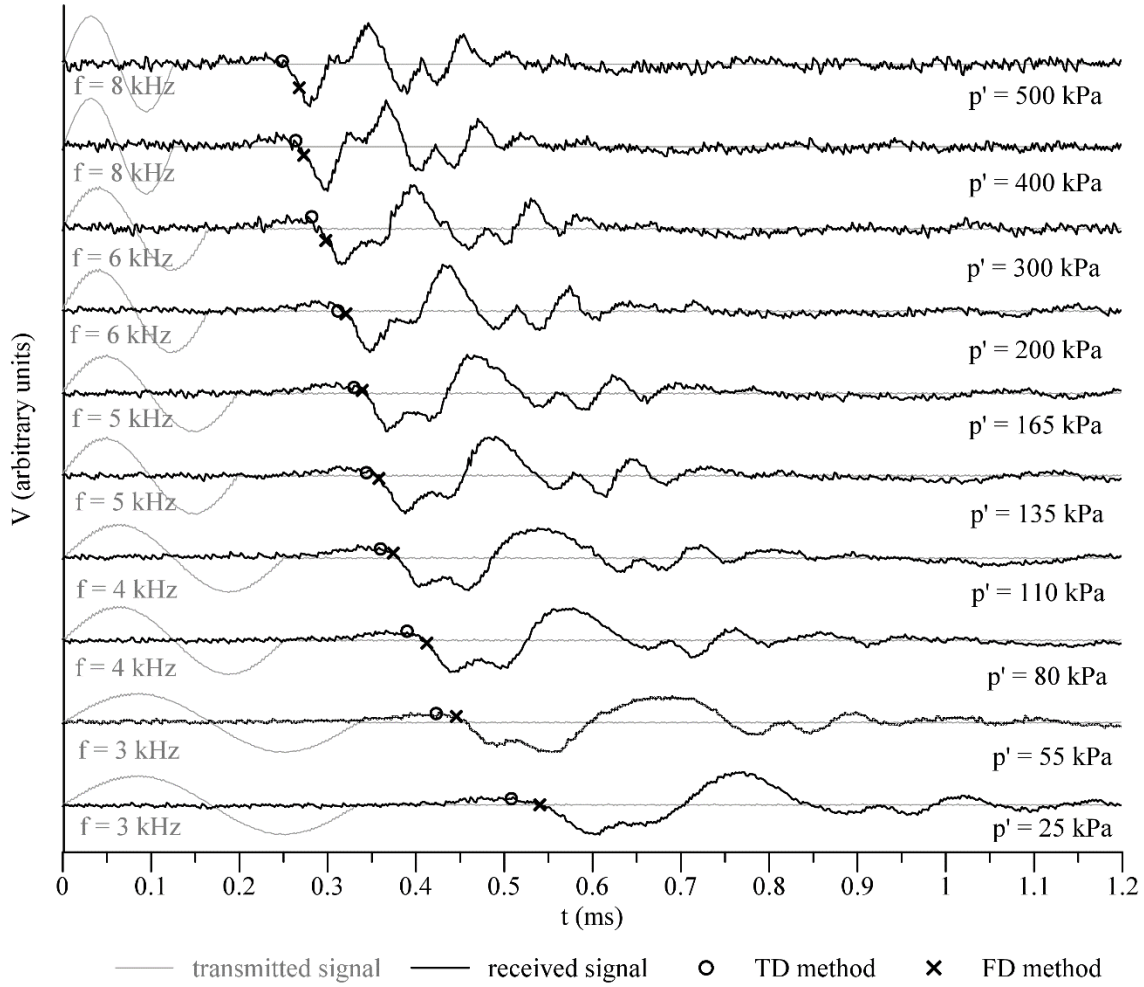


Fig. 3. Selected first arrivals in time-domain (TD) and in frequency-domain (FD) at the selected stress levels, during the first loading of the ICDIC 0.794/25 test

The results of the frequency domain (FD) methodology are also plotted in Fig. 3, showing that higher arrival times were always obtained when using the FD method, as previously reported by Viggiani and Atkinson (1995), Greening and Nash (2004) and Alvarado and Coop (2011). Some of the arrival times estimated by the FD method are located within the middle part of the sine pulse (e.g. output signals corresponding to p' = 300, 400 and 500 kPa) and, consequently, seem to represent less accurately the shear-wave arrivals. Since similar conclusions were reached when analysing the results of the BE tests performed during the ICDIC 0.659/25, it was decided to disregard the arrival times estimated by the FD method and adopt those estimated by the TD method.

The values of the small-strain shear modulus, G_{max}, obtained for the ICDIC 0.794/25 and ICDIC 0.659/25 tests during the first loading (1L), the first unloading (1UL), the reloading (2L) and the second unloading (2UL) stages are presented in Fig. 4. As expected, the estimated values of G_{max} are higher for the denser specimen (ICDIC 0.659/25 test). Moreover, it seems that overconsolidation has little influence on the small-strain behaviour of Hostun sand. As discussed by Zhou and Chen (2005), for sands subjected to very low strain amplitude cyclic loading under static confinement, the effect of the previous stress history on G_{max} is not significant, thus G_{max} can be essentially related to the mean effective stress and the void ratio.

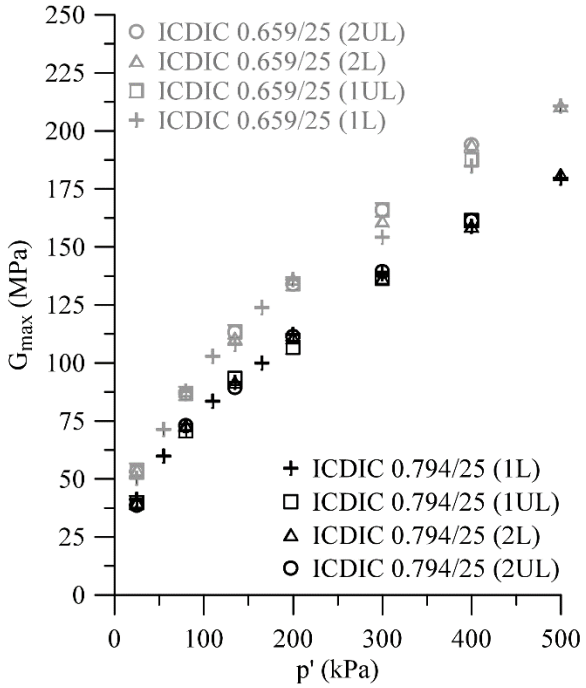


Fig. 4. Values of the small-strain shear modulus estimated using the first arrival (time-domain) method for the ICDIC 0.794/25 and ICDIC 0.659/25 tests

Results of all BE tests were used to calibrate the following expression, proposed by Hardin (1978):

$$G_{max} = C_g \; p'_{ref} \; f(e) \; OCR^k \left(\frac{p'}{p'_{ref}} \right)^{n_g} \tag{2}$$

where C_g, n_g and k are soil-dependent constants, p'_{ref} is the reference pressure (atmospheric pressure), OCR is the overconsolidation ratio and f(e) is a function of the void ratio. The value of k was set to 0, due to the aforementioned very slight effect of overconsolidation on G_{max}. With respect to f(e), the following expression proposed by Hardin and Richart (1963) for angular-grained sands was used:

$$f(e) = \frac{(2.97 - e)^2}{1 + e} \tag{3}$$

The application of this procedure to the BE data obtained from ICDIC 0.794/25 and ICDIC 0.659/25 tests is illustrated in Fig. 5.

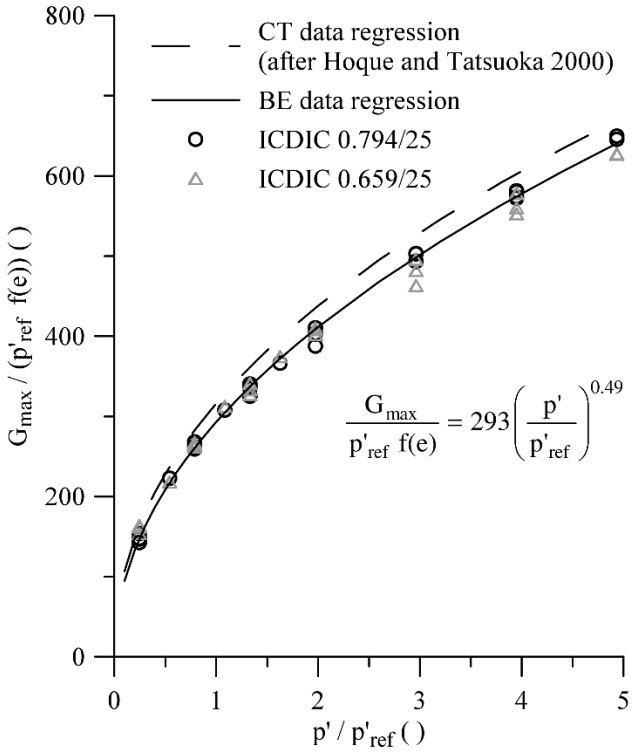


Fig. 5. Small-strain shear modulus for Hostun sand

It can be observed that results present little scatter, being adequately reproduced by Equation (2) when C_g and n_g are set to 293 and 0.49, respectively. It is also noteworthy that results of this study are only about 5 – 10 % lower than those reported by Hoque and Tatsuoka (2000), which were obtained using small-amplitude cyclic triaxial loading (CT) on Hostun sand.

Behaviour of Hostun sand within the medium to large strain range

Fundamental concepts

In order to comprehensively analyse the drained and undrained triaxial compression and extension test results performed on air-pluviated Hostun sand, three distinctive states of the behaviour of sand are examined: the phase transformation state (PTS), the peak stress ratio state (PSRS) and the critical state (CS). The PTS and the PSRS are both transitory states of sand behaviour, which can occur either at moderate strains or large strains, depending on the density and stress state (e.g. Been and Jefferies 1985; Jefferies and Been 2006). While the PTS is the state at which the behaviour of sand changes from plastic contraction to plastic dilation (i.e. the dilatancy is temporarily null), the PSRS is related to the mobilisation of the maximum angle of shearing resistance. With respect to the CS, it is defined as the state established at large strains at which the soil deforms under constant stress and void ratio (Roscoe *et al*. 1958). This state has been widely used as a reference state for constitutive modelling, influencing almost every characteristic of soil behaviour. Therefore, particular attention is firstly given in this paper to the reliable prediction of the CS. Subsequently, the occurrence of both the PSRS and PTS are assessed as a function of the state parameter.

Lastly, the stress-dilatancy behaviour of air-pluviated Hostun sand is examined, as its accurate description has been recognised as a crucial issue for the accurate modelling of the stress-strain behaviour of sand (Li and Dafalias 2000; Jefferies and Been 2006).

Critical state

Although a significant number of tests were conducted, critical state conditions appear to be only attained in four tests. For the remaining tests, clear signs of stresses and volumetric strain stabilisation – for drained shearing – or stresses and pore water pressure stabilisation – for undrained shearing – are not visible and, consequently, the conditions at the end of those tests cannot be considered as representative of CS.

Fig. 6 shows results of four drained TC tests and one drained TE test performed on samples subjected to the same isotropic consolidation stress (σ'_0 = 80 kPa), but having different initial void ratios. As expected, the obtained monotonic response of sand depends greatly on the initial void ratio, as well as on the stress path imposed in each test. More specifically, when comparing the stress-strain responses of samples subjected to similar loading paths – ICDMTCp↑ 0.885/80, ICDMTCp↑ 0.798/80 and ICDMTCp↑ 0.725/80 (Fig. 6a) –, it can be observed that a higher peak strength is obtained for denser samples at lower strain levels, as expected. Moreover, it can be seen that denser samples tend to contract less during the initial stages of loading and start dilating at lower strain levels (Fig. 6b). For the tests listed above, a stabilisation of both $q - \varepsilon_a$ and $\varepsilon_v - \varepsilon_a$ responses at large strains seems to occur only for the loosest sample (i.e. ICDMTCp↑ 0.885/80).

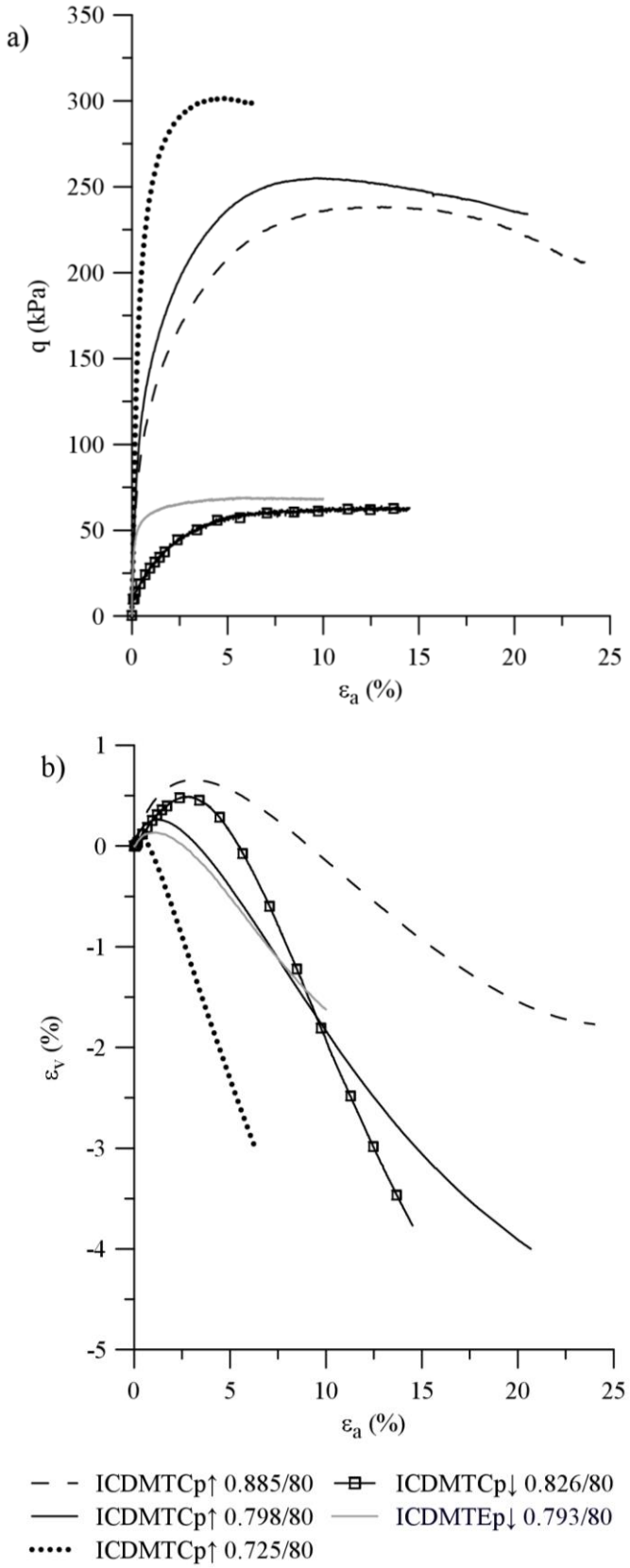


Fig. 6. Drained TC and TE tests with p'_0 = 80 kPa: (a) stress-strain and (b) volumetric strain as a function of the axial strain

It is also interesting to compare the results of the ICDMTCp↑ 0.798/80 and ICDMTCp↓ 0.826/80 tests presented in that figure, even if the initial void ratios of these samples were slightly different. As can be seen, considerably lower strength and stiffness were obtained for the test with decreasing mean stress (ICDMTCp↓ 0.826/80). Similar results were reported by Vaid and Sasitharan (1992) on water-pluviated Erksak sand.

Fig. 6 also compares the behaviour of similarly prepared samples when subjected to drained TC and TE – ICDMTCp↑ 0.798/80 and ICDMTEp↓ 0.793/80 tests, respectively. Even if a higher volumetric contraction was measured in the TC test (Fig. 6b), a softer and less-resistant response was obtained for the sample subjected to TE (Fig. 6a). A similar behaviour was reported by Bianchini *et al.* (1991) for dense Hostun sand, tested on a hollow cylinder torsional apparatus and on a cubic cell device. Moreover, these results are in a remarkable good agreement with those obtained when shearing Hostun sand under undrained conditions (Fig. 7). Although smaller positive excess pore water pressure was generated in the ICUMTEp↓ 0.839/80 test (Fig. 7c), when compared with that developed in the ICUMTCp↑ 0.801/80 test, a higher reduction of the mean effective stress was obtained for the TE test (Fig. 7a), as expected (e.g. Miura and Toki 1982; Yoshimine *et al.* 1998). Moreover, a softer response can be observed for the ICUMTEp↓ 0.839/80 test (Fig. 7b). Similar results were also obtained for very loose Hostun sand by Doanh *et al.* (1997).

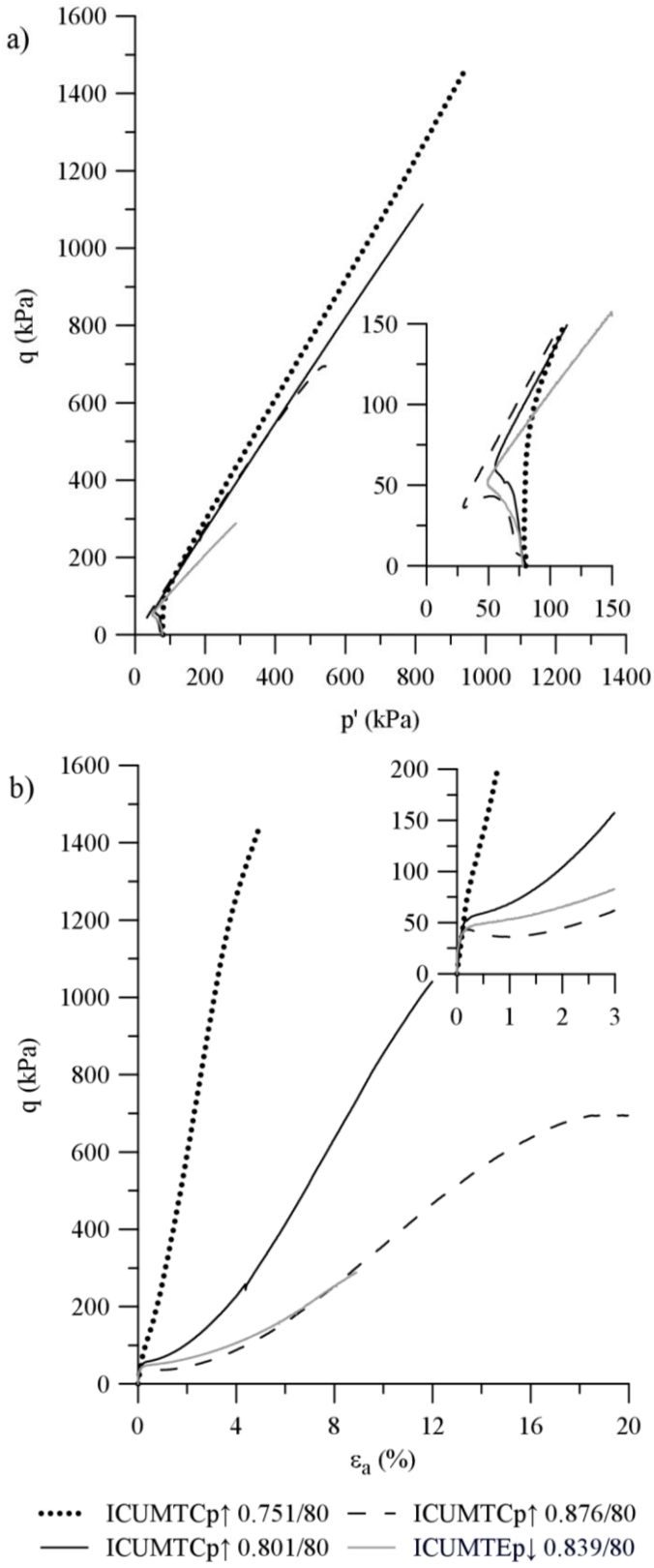


Fig. 7. Undrained TC and TE tests with p'_0 = 80 kPa: (a) stress path, (b) stress-strain behaviour and (c) pore water pressure evolution with strain

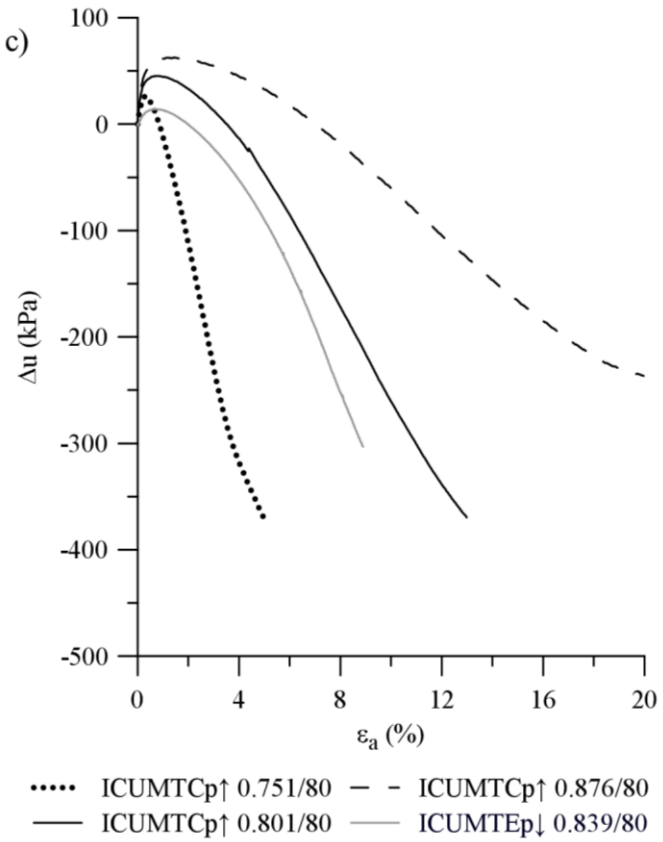


Fig. 7. Undrained TC and TE tests with p'0 = 80 kPa: (a) stress path, (b) stress-strain behaviour and (c) pore water pressure evolution with strain (cont.)

The void ratio – mean effective stress data at the end of all drained and undrained TC tests conducted on initially loose and moderately loose specimens are illustrated in Fig. 8. For those tests where CS conditions were not attained (unfilled markers), arrows indicate the directions of the paths at the instant when those tests were stopped. It can be observed that it was not possible to obtain data representative of CS at low stresses (below 100 kPa). According to Klotz and Coop (2002), this difficulty may arise from the incompleteness of tests, as a consequence of the premature occurrence of barrelling and strain localisation when samples are sheared under lower confining stresses. This problem seems to be particularly evident when pluviation is used to prepare samples, since it is practically impossible to prepare initially looser than critical state samples at stress levels in the range of 0 – 1000 kPa (as it was the case of the present study) and, consequently, the critical state line in this range can only be reached by drained triaxial tests on dilatant samples (Been *et al.*, 1991).

As proposed by Li and Wang (1998), a power law was used to define the critical state line (CSL):

$$e_{CS} = e_{0;ref} - \lambda \left(\frac{p'}{p'_{ref}} \right)^{\xi} \quad (4)$$

where $e_{0;\,ref}$, λ and ξ are fitting parameters, which were estimated by the least-squares regression. Due to the aforementioned difficulty in obtaining CS data at low stresses, the void ratio under zero effective stress, $e_{0;\,ref}$, was constrained by the maximum void ratio, e_{max}, as proposed by Riemer *et al.* (1990) and also assumed in subsequent studies (Klotz and Coop 2002; Murthy *et al.* 2007). By employing that approach, values of 1.00, 0.07 and 0.36 were estimated for $e_{0;\,ref}$, λ and ξ, respectively, with the resulting critical state line (CSL) being depicted in Fig. 8.

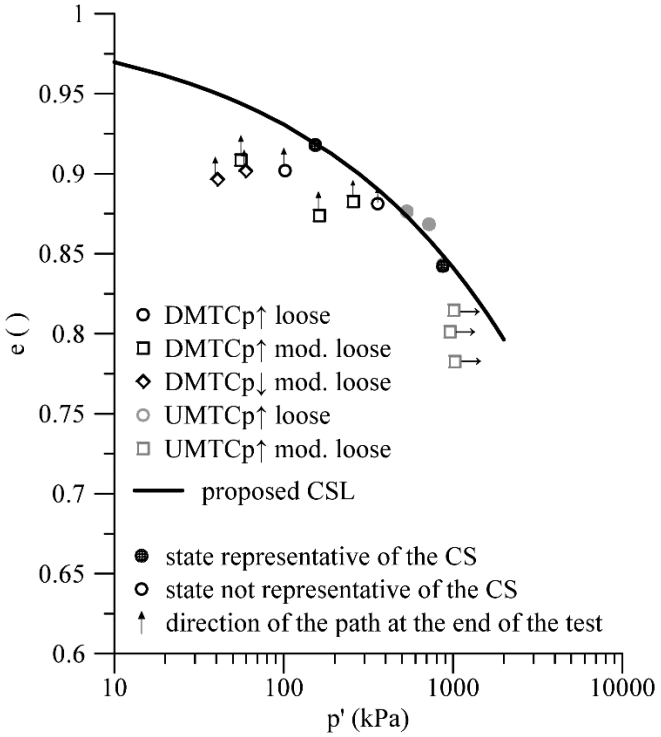


Fig. 8. Prediction of the critical state line for Hostun sand

The obtained CS data were subsequently compared with other results of TC tests on Hostun sand presented in the literature (Table 3). It can be seen in Fig. 9 that the additional data found

in the literature plot very close to the CSL proposed in this paper, independently of the sample preparation method.

Table 3. Characteristics of TC tests performed on Hostun sand at other institutions and used for comparing with the results obtained by the authors

Test ID †	Method of prep.§	e_0 ( )	p'_0 (kPa)	ψ_0 ( )	$e_{end\ test}$ ( )	$p'_{end\ test}$ (kPa)	Institution	Reference
ICDMTCp↑ 0.867/600	AP	0.867	600	-0.030	0.820	933.4	INPG (*)	Desrues and Mokni (2007)
ICUMTCp↑ 0.895/300	AP	0.895	300	0.000	0.895	205.3	INPG (*)	Desrues and Mokni (2007)
ICUMTCp↑ 0.970/279	MT	0.970	279	0.072	0.970	22.0	INPG (*)	Konrad (1993)
ICUMTCp↑ 0.922/772	MT	0.922	772	0.063	0.922	60.1	INPG (*)	Konrad (1993)
ICDMTCp↑ 0.918/100	MT	0.918	100	-0.009	0.908	173.5	ENPC (**)	Benahmed (2001)
ICDMTCp↑ 0.910/200	MT	0.910	200	0.001	0.887	345.1	ENPC (**)	Benahmed (2001)
ICDMTCp↑ 0.899/400	MT	0.899	400	0.013	0.859	682.3	ENPC (**)	Benahmed (2001)
ICUMTCp↑ 0.919/100	MT	0.919	100	-0.008	0.919	103.9	ENPC (**)	Benahmed (2001)
ICUMTCp↑ 0.910/200	MT	0.910	200	0.001	0.910	154.1	ENPC (**)	Benahmed (2001)
ICUMTCp↑ 0.898/400	MT	0.898	400	0.012	0.898	216.3	ENPC (**)	Benahmed (2001)

Note: † The designation is identical to that presented in Table 2 (see note below that table).

§ Method of sample preparation: air-pluviation (AP) or moist tamping (MT).

(*) Grenoble Institute of Technology (INPG); (**) *École Nationale des Ponts et Chaussées* (ENPC).

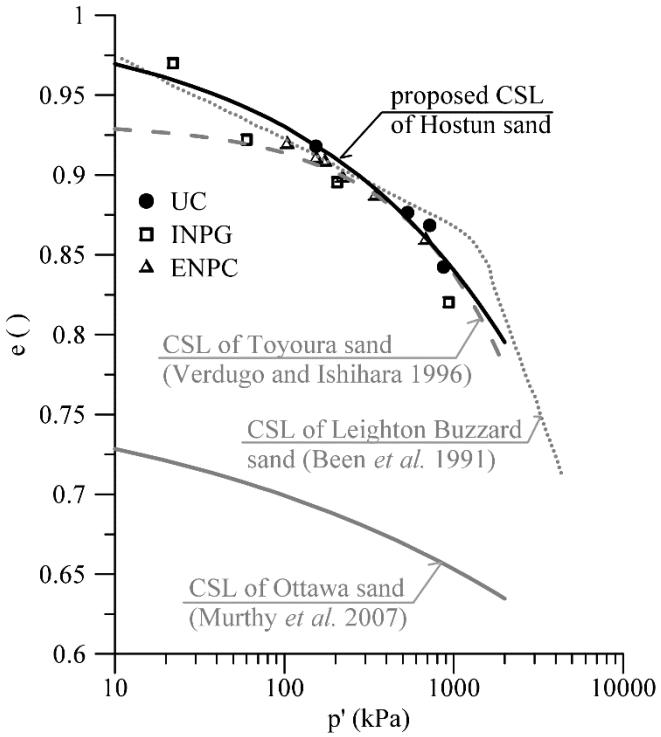


Fig. 9. Comparison of the proposed critical state line (CSL) with results presented in the literature

Additionally, Fig. 9 presents the CSL proposed for Toyoura sand (Verdugo and Ishihara 1996), Leighton Buzzard sand (Been *et al.* 1991) and Ottawa sand (Murthy *et al.* 2007). Interestingly, as previously discussed by Klotz and Coop (2002), it was found that the CSL proposed for sands with identical particle shape (namely, Hostun, Toyoura and Leighton Buzzard sands, as indicated in Table 1) plot very close to each other for values of p' within the range of 100 to 1000 kPa, despite having different particle size distributions (Fig. 1). Conversely, although presenting similar particle size distributions, the CSL proposed for Ottawa sand is located far below that suggested for Hostun sand. This suggests that particle shape has a major influence on the CSL of sand (particularly in $e_{0;\,ref}$), as proposed by Cho *et al.* (2006).

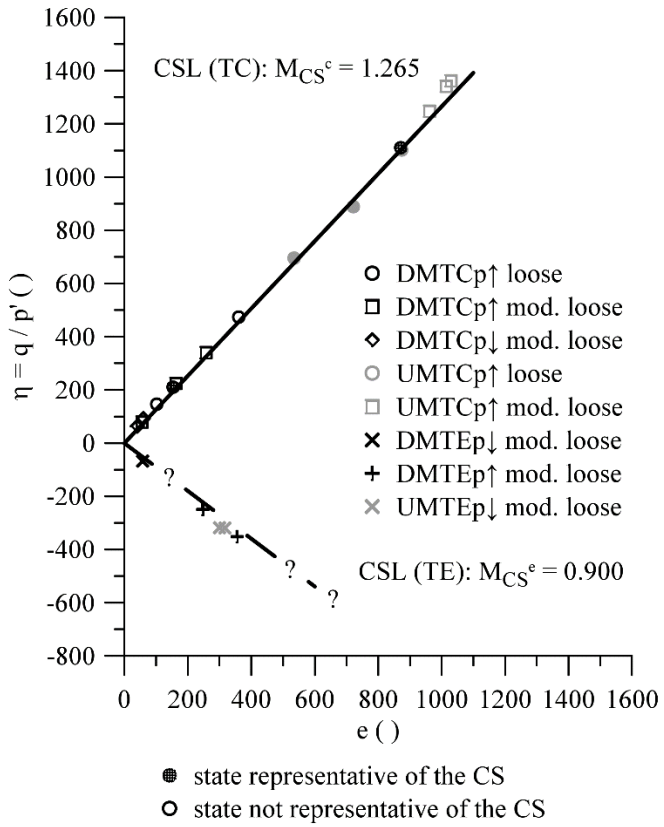


Fig. 10. Critical state strength of Hostun sand in compression and in extension

The CS strength in triaxial compression and triaxial extension, identified by superscripts "c" and "e", respectively, is quantified by the corresponding stress ratio $M_{CS}^{c,e} = (q/p')_{CS}$. Fig. 10 presents the q – p' data obtained at the end of shearing for loose and moderately loose specimens. The four points which were considered representative of the CS are distinguished by using filled markers. Based on these CS points, the critical strength in TC, M_{CS}^{c}, was estimated as 1.265, which corresponds to a CS friction angle, ϕ_{CS}^{c}, of approximately 31.5º.

With respect to the CS in TE, it is difficult to obtain a reliable estimation from the obtained results, since test data measured after the occurrence of necking were disregarded. Several experimental studies have shown that the friction angle in TE, ϕ_{CS}^{e}, is close to ϕ_{CS}^{c} for pluviated sands (e.g. Vaid *et al.* 1990; Lade 2006). In the present study, a stress ratio M_{CS}^{e} of 0.90 was considered, corresponding to ϕ_{CS}^{e} of 32º and to a ratio M_{CS}^{e}/M_{CS}^{c} of about 0.71,

which is within the typical 0.67-0.75 range for silica sands (Loukidis and Salgado 2009). The q – p' values corresponding to the moment immediately before necking was observed are plotted in Fig. 10. These points does not plot far from the adopted CS strength line in extension.

Peak stress ratio state

The occurrence of a peak stress ratio, η_{PSRS}, can be related to the current value of the state parameter, ψ, through the following equation (Wood *et al.* 1994):

$$\eta_{PSRS}^{c,e} = M_{CS}^{c,e} - k_{PSRS}^{c,e} \psi_{PSRS} \quad (5)$$

where $k_{PSRS}^{c,e}$ is a set of material constants (one value for compression and another for extension). This relationship has been incorporated in several constitutive models for sands (e.g. Manzari and Dafalias 1997), even if some authors have subsequently replaced the linear dependency on the state parameter by an exponential variation (e.g. Li and Dafalias 2000).

Fig. 11 shows η_{PSRS} plotted against ψ_{PSRS} for all tests performed. Irrespective of the type of consolidation, of the drainage conditions and of the stress-path direction, the experimental results are well represented by an equation of the form of (5). The fitting parameters $k_{PSRS}^{c,e}$ were obtained by employing the least-square method and are indicated in the figure. In TE, a slope ($k_{PSRS}^{e} = 1.66$) slightly lower than that commonly assumed in constitutive modelling $k_{PSRS}^{e} = \left(M_{CS}^{e} / M_{CS}^{c}\right) k_{PSRS}^{c} = 2.00$ (e.g. Papadimitriou and Bouckovalas 2002) was found. It is also interesting to note that the results do not seem to suggest that there could be any substantial gain in accuracy by introducing an exponential relationship between the peak stress ratio and the stress ratio at critical state.

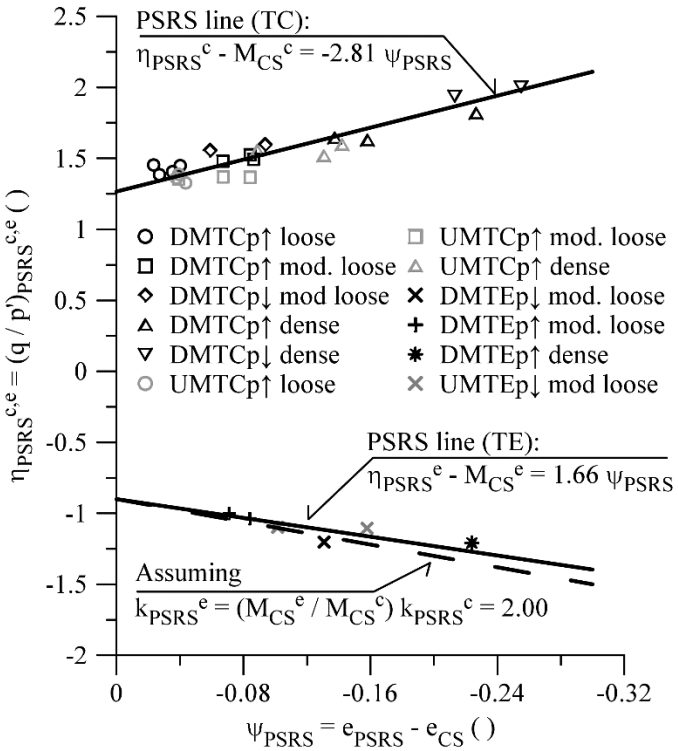


Fig. 11. Peak stress ratio as a function of the state parameter

Phase transformation state

Under undrained conditions, the phase transformation state (PTS) can be associated with a local minimum in the mean effective stress, p' (Ishihara *et al.* 1975). In the case of drained shearing, the identification of the PTS is much more complex, since the estimation of the dilatancy coefficient, D, and consequently of the plastic volumetric, ε_v^p, and deviatoric, ε_q^p, strains have to be performed. For that purpose, a forward-difference first-order approach, similar to that outlined by Been and Jefferies (2004), was employed:

$$D = \frac{d\varepsilon_v^p}{d\varepsilon_q^p} \approx \frac{\delta\varepsilon_v - \delta\varepsilon_v^e}{\delta\varepsilon_q - \delta\varepsilon_q^e} \approx \frac{\left(\varepsilon_{v_{j+1}} - \varepsilon_{v_j}\right) - \left(p'_{j+1} - p'_j\right) / K_{tan}}{\left(\varepsilon_{q_{j+1}} - \varepsilon_{q_j}\right) - \left(q_{j+1} - q_j\right) / \left(3\,G_{tan}\right)} \qquad (6)$$

where the tangent bulk, K_{tan}, and shear, G_{tan}, moduli were assumed constant for each step j. The expression above assumes an isotropic hypoelastic formulation and, as a result, that the deviatoric and volumetric elastic response are decoupled. In particular, both moduli are a function of the mean effective stress (see Equation (2)), since, as a simplification, their values

were assumed to be equal to their small-strain values (i.e. $K_{tan} = K_{max}$ and $G_{tan} = G_{max}$). While frequently employed when interpreting sand behaviour (e.g. Been and Jefferies 2004; Loukidis and Salgado 2009), it has been established that such approach does not observe the laws of thermodynamics and may lead to unconservative results (see Houlsby *et al.* (2005) for further details on this issue). Moreover, given that only G_{max} was measured directly using bender element testing, the value of K_{max} was obtained using the elastic relationship:

$$K_{max} = \frac{2(1+\nu)}{3(1-2\nu)} G_{max} \tag{7}$$

where a constant Poisson's ratio, ν, equal to 0.18 (Hoque and Tatsuoka 2000) was assumed. As discussed by Loukidis and Salgado (2009), the assumption that $K_{tan} = K_{max}$ and $G_{tan} = G_{max}$ is an acceptable approximation when data from drained tests are used. Since deformations in sand are predominantly of plastic nature when subjected to triaxial loading, results of Equation (6) are primarily affected by the measured total volumetric, ε_v, and deviatoric, ε_q, strains. Thus, the influence of K_{tan} and G_{tan} on the estimation of D is small when analysing the drained response of the material. Conversely, under undrained conditions, $\delta\varepsilon_v = 0$ and, consequently, D is strongly influenced by $\delta\varepsilon_v^e \approx \left(p'_{j+1} - p'_j\right) / K_{tan}$.

Similar to the description of the PSR state, a dependence of the stress ratio at PTS, η_{PTS}, on the current value of the state parameter, ψ, with reference to the CS, was proposed by Manzari and Dafalias (1997):

$$\eta_{PTS}^{c,e} = M_{CS}^{c,e} + k_{PTS}^{c,e} \psi_{PTS} \tag{8}$$

where $k_{PTS}^{c,e}$ is a new set of material constants.

Fig. 12 shows η_{PTS} plotted against ψ_{PTS} for all conducted tests. Although some scatter exists, results support the trend suggested by Equation (8), as previously reported for other sands, such as Toyoura sand (Loukidis and Salgado 2009) and Ottawa sand (Murthy *et al.* 2007). The

material constants $k_{PTS}^{c,e}$ were obtained through the use of least-square regressions over all available test data, resulting in 0.94 and -0.10 for compression and extension loading conditions, respectively. Similar to the conclusions drawn when analysing the PSRS data, the constant used to predict the occurrence of the PTS under TE loading ($k_{PTS}^{e} = -0.10$) diverges slightly from that commonly assumed ($k_{PTS}^{e} = \left(M_{CS}^{e} / M_{CS}^{c}\right) k_{PTS}^{c} = -0.67$).

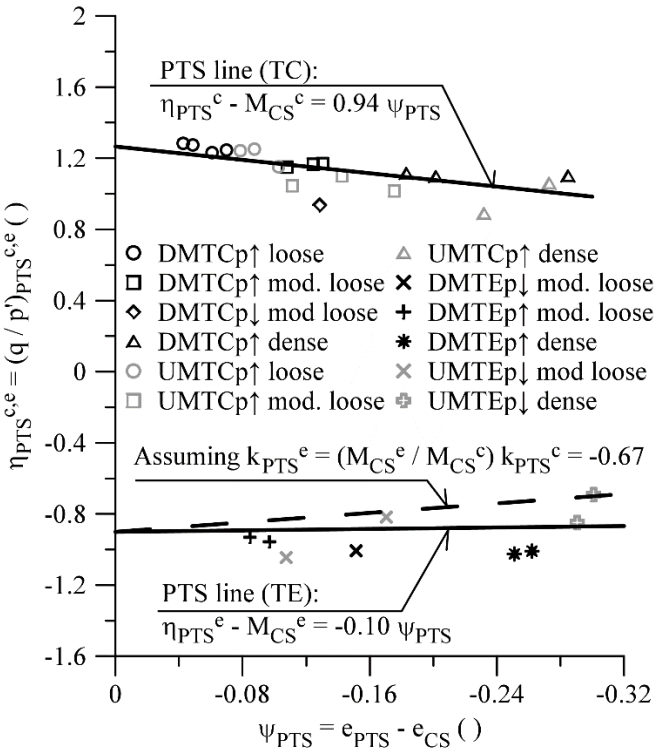


Fig. 12. Stress ratio at phase transformation state as a function of the state parameter

Stress-dilatancy characteristics

Within the several proposals existing in the literature, it is of special interest here to analyse the stress-dilatancy relationship introduced by Manzari and Dafalias (1997), which is widely used in constitutive modelling of sands:

$$D = A_d (\eta_{PTS} - \eta) \tag{9}$$

where A_d is a model constant. This equation states a direct dependence of the dilatancy rate, D, on the difference between the current stress ratio, η, and the stress ratio at PTS, η_{PTS}. Since this

latter parameter depends on the current state of sand (as suggested by Equation (8) and clearly corroborated by the experimental data presented in Fig. 12), Equation (9) introduces D as a state-dependent quantity.

Fig. 13 shows the stress-dilatancy curves obtained from the available TC data. It seems that Equation (9) can be used to adequately describe the stress-dilatancy behaviour of both loose and dense samples, at least until η_{PSRS} is reached.

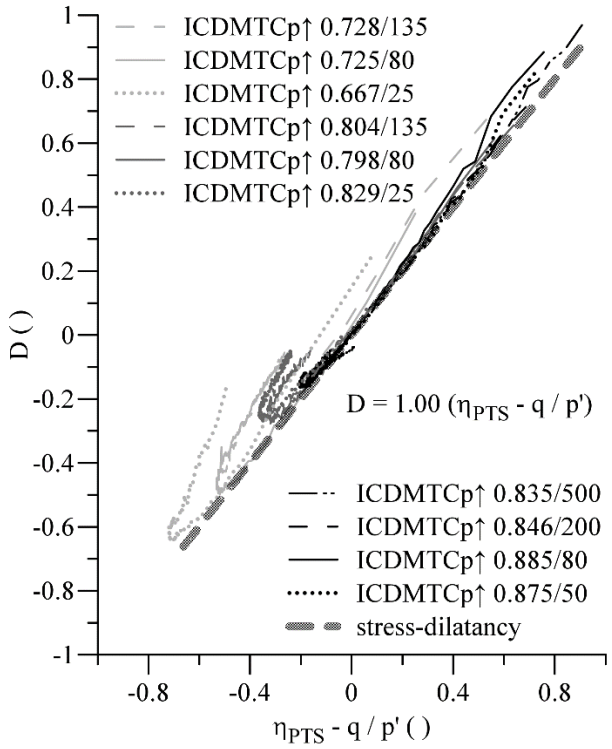


Fig. 13. Stress-dilatancy relationship determined from drained TC tests

Conclusions

An extensive laboratory testing programme has been performed on air-pluviated Hostun sand to examine its behaviour under a wide range of strains. Results of BE tests performed on moderately loose and dense specimens were used to estimate the shear modulus at small-strains. As expected, the behaviour within this strain range can be primarily related to the current void ratio and mean effective stress.

Within the medium to large strain range, a state parameter approach was used in conjunction with the critical state framework to assess the distinctive states of the monotonic response of

air-pluviated Hostun sand, namely the critical state (CS), the peak stress ratio state (PSRS) and the phase transformation state (PTS). Results of drained and undrained tests conducted on loose samples were used for the prediction of the critical state line (CSL). Additional test data found in the literature was used to corroborate the proposed CSL, which appears to be independent of the sample preparation method and drainage conditions.

Irrespective of the stress state and void ratio after consolidation, the drainage conditions and the stress-path direction, the PSRS and the PTS deducted from the experimental results appear to be very well described by simple linear state-dependent relationships. For drained shearing, the detection of the PTS required the direct estimation of the dilatancy and consequently of the plastic strains. Despite the complexity associated to that calculation and the simplifications assumed, a remarkable correlation between the stress ratio at phase transformation and the current state parameter was obtained. Furthermore, it was found that the dilatancy deduced from drained triaxial compression tests conducted on both loose and dense samples can be adequately associated to the difference between the current stress ratio and the stress ratio at the phase transformation as proposed in the literature.

The large amount of laboratory test results presented in this paper intends to provide reliable data for the calibration of advanced constitutive models based on a critical state framework to be used in numerical analysis, as well as to clarify aspects of complex geotechnical problems identified in centrifuge modelling, including but not limited to liquefaction mechanisms. In addition, the systematic procedure for interpreting the obtained experimental data can be used as a reference for characterising other sands in the future.

Acknowledgements

This research has been financially supported by FCT – Fundação para a Ciência e Tecnologia, Portugal, through Research Project PTDC/ECM/103220/2008. The first author is also funded through FCT's grant no. SFRH/BD/84656/2012, as part of the financial programme POPH –

Programa Operacional Potencial Humano, which he gratefully acknowledges. The authors would also like to thank Dr. A. Pedro of the University of Coimbra for his precious assistance in performing and interpreting bender element tests, as well as Professor J. Desrues for making available the experimental data from triaxial tests carried out at the Grenoble Institute of Technology.

List of symbols

The following symbols are used in this paper:

A_d = dilatancy constant – parameter defining the stress-dilatancy relationship;

c = ratio between critical state strength in triaxial extension and compression;

C_g, n_g, k = parameters defining the influence of the void ratio, overconsolidation ratio and mean effective stress on the small-strain shear modulus (Equation 2);

C_u = uniformity coefficient;

D = dilatancy coefficient;

D_{50} = mean particle diameter;;

e = void ratio;

e_0, e_{CS}, $e_{end\ test}$, e_{PSRS}, e_{PTS} = void ratio, e, after consolidation, at critical state, at end of the test, at peak stress ratio state and at phase transformation state, respectively;

$e_{0;ref}$, λ, ξ = parameters defining the position of the critical state line (Equation 4);

e_{min}, e_{max} = minimum and maximum void ratios, respectively;

f = input frequency of excitation (bender element tests);

f(e) = function of the void ratio;

G_{max} = maximum (or small-strain) shear modulus;

G_s = density of soil particles;

G_{tan} = tangent shear modulus;

K_{max} = maximum (or small-strain) bulk modulus;

$k^{c,e}_{PSRS}$ = parameters defining the position of the peak stress ratio state line (Equation 5);

$k^{c,e}_{PTS}$ = parameters defining the position of the phase transformation state line (Equation 6);

L = travel distance of shear wave;

M^{c}_{CS}, M^{e}_{CS} = stress ratio at critical state in compression and in extension, respectively;

OCR = overconsolidation ratio;

p = mean total stress;

p' = mean effective stress;

p'_0, $p'_{end\ test}$, p'_{PSRS}, p'_{PTS} = mean effective stress after consolidation, at end of the test, at peak stress ratio state and at phase transformation state, respectively;

p'_{ref} = reference pressure;

q = deviatoric stress;

$q_{end\ test}$, q_{PSRS}, q_{PTS} = deviatoric stress at end of the test, at peak stress ratio state and at phase transformation state, respectively;

t = travel time of shear wave;

V = normalised voltage;

V_s = shear-wave velocity;

ε_a, ε_q, ε_r, ε_v = axial, deviatoric, radial and volumetric strains, respectively;

$\delta\varepsilon_q$, $\delta\varepsilon^{e}_{q}$, $\delta\varepsilon^{p}_{q}$ = total, elastic and plastic volumetric strain increments, respectively;

$\delta\varepsilon_v$, $\delta\varepsilon^{e}_{v}$, $\delta\varepsilon^{p}_{v}$ = total, elastic and plastic volumetric strain increments, respectively;

ϕ^{c}_{CS}, ϕ^{e}_{CS} = angle of friction at critical state in compression and in extension, respectively;

η = stress ratio;

$\eta_{end\ test}$, η_{PSRS}, η_{PTS} = stress ratio at end of the test, at peak stress ratio state and at phase transformation state, respectively;

ν = Poisson's ratio;

ρ = mass density;

ψ = state parameter ($\psi = e - e_{CS}$);

ψ_0, ψ_{PSRS}, ψ_{PTS} = state parameter, ψ, after consolidation, at peak stress ratio state and at phase transformation state, respectively.

References

Alvarado, G. and Coop, M. R. (2011). "On the performance of bender elements in triaxial tests". *Géotechnique*, 62(1), 1–17.

Arulnathan, R., Boulanger, R. S. and Riemer, M. F. (1998). "Analysis of bender element tests". *Geotech. Test. J.*, 21(2), 120–131.

American Society for Testing and Materials (ASTM). (2006). "Standard test methods for maximum index density and unit weight of soils using a vibratory table". *D4253-00*, ASTM International, West Conshohocken, PA, USA.

American Society for Testing and Materials (ASTM). (2006). "Standard test methods for minimum index density and unit weight of soils and calculation of relative density". *D4254-00*, ASTM International, West Conshohocken, PA, USA.

Baldi, G. and Nova, R. (1984). "Membrane penetration effects in triaxial testing". *J. Geotech. Eng.*, 10.1061/(ASCE)0733-9410(1984)110:3(403), 403–420.

Been, K., and Jefferies, M. G. (1985). "A state parameter for sands". *Géotechnique*, 35(2), 99–112.

Been, K. and Jefferies, M. G. (2004). "Stress-dilatancy in very loose sand". *Can. Geotech. J.*, 41, 972–989.

Been, K., Jefferies, M. G. and Hachey, J. (1991). "The critical state of sands". *Géotechnique*, 41(3), 365–381.

Been, K., Lingnau, B. E., Crooks, J. H. A. and Leach, B. (1987). "Cone penetration test calibration for Erksak (Beaufort Sea) sand". *Can. Geotech. J. 24, 601-610*.

Benahmed, N. (2001). *Comportement mécanique d'un sable sous cisaillement monotone et cyclique : application aux phénomènes de liquéfaction et de mobilité cyclique*. Ph.D. dissertation, École Nationale des Ponts et Chaussées, Paris, France *(in French)*.

Bianchini, G., Saada, A., Puccini, P., Lanier, J. and Zitouni, Z. (1991). "Complex stress paths and validation of constitutive models". *Geotech. Test. J.*, 14(1), 13–25.

Bishop, A. W. and Wesley, L. D. (1975). "A hydraulic triaxial apparatus for controlled stress path testing". *Géotechnique*, 25(4), 657–670.

Chian, S.C., Tokimatsu, K. and Madabhushi, S.P.G. (2014). “Soil liquefaction-induced uplift of underground structures: Physical and numerical modeling”. *J. Geotech. Geoenviron. Eng.*, , 10.1061/(ASCE)GT.1943-5606.0001159, 04014057.

Cho, G.-C., Dodds, J. and Santamarina, J. C. (2006). “Particle shape effects on packing density, stiffness, and strength: natural and crushed sands”. *J. Geotech. Geoenviron. Eng.*, 10.1061/(ASCE)1090-0241(2006)132:5(591), 591–602.

Coelho, P.A.L.F. (2007). *In situ densification as a liquefaction resistance measure for bridge foundation*. Ph.D. dissertation, Univ. of Cambridge, Cambridge, U.K.

De Gennaro, V., Canou, J., Dupla, J. C. and Benahmed, N. (2004). “Influence of loading path on the undrained behaviour of a medium loose sand”. *Can. Geotech. J.*, 41, 166–180.

Desrues, J., Chambon, R., Mokni, M. and Mazerolle, F. (1996). “Void ratio evolution inside shear bands in triaxial sand specimens studied by computed tomography”. *Géotechnique*, 46(3), 529–546.

Desrues, J. and Mokni, M. (2007). “Drained and undrained biaxial test data on Hostun RF sand”. http://geo.hmg.inpg.fr/desrues/doalert/. (July, 24, 2014).

Doanh, T., Ibraim, E. and Matiotti, R. (1997). “Undrained instability of very loose Hostun sand in triaxial compression and extension. Part 1: experimental observations”. *Mech. Cohesive-Frictional Mat.*, 2, 47–70.

Dyvik, R. and Madshus, C. (1985). “Lab measurements of Gmax using bender elements”. *Proc., ASCE Annual Convention, Advances in the art of testing soils under cyclic conditions*, Detroit, Michigan, 186–197.

Flavigny, E., Desrues, J. and Palayer, B. (1990). “Le sable d’Hostun «RF»”. *Revue Française de Géotechnique*, 53, 67–69.

Gajo, A. and Muir Wood, D. (1999). “Severn–Trent sand: a kinematic-hardening constitutive model: the q–p formulation”. *Géotechnique*, 49(5), 595–614.

Greening, P. D. and Nash, D. F. T. (2004). “Frequency domain determination of G0 using bender elements”. *Geotech. Test. J.*, 27(3), 288–294.

Hardin, B. O. and Richart, F. E. (1963). “Elastic wave velocities in granular soils”. *J. Soil Mech. Found. Div.*, 89(1), 33–65.

Hardin, B. O. (1978). “The nature of stress-strain behavior of soils”. *Proc., ASCE Geotech. Eng. Div. Specialty Conf.*, Pasadena, 1, 3–90.

Hoque, E. and Tatsuoka, F. (2000). “Kinematic elasticity of a granular material”. *Proc., GeoEng 2000, Melbourne*.

Houlsby, G. T., Amorosi, A. and Rojas, E. (2005). "Elastic moduli of soils dependent on pressure: a hyperelastic formulation". *Géotechnique*, 55(5), 383–392.

Ishihara, K. (1993). “Liquefaction and flow failure during earthquakes”. *Géotechnique*, 43(3), 351–451.

Ishihara, K., Tatsuoka, F. and Yasuda, S. (1975). “Undrained deformation and liquefaction of sand under cyclic stresses”. *Soils Found.*, 15(1), 29–44.

Jefferies, M. G. and Been, K. (2006). *Soil liquefaction: a critical state approach*. Taylor and Francis e-Library.

Klotz, E. U., and Coop, M. R. (2002). “On the identification of critical state lines for sands”. *Geotech. Test. J.*, 25(3), 1–14.

Konrad, J.-M. (1993). “Undrained response of loosely compacted and cyclic compression sands during monotonic tests”. *Géotechnique*, 43(1), 69–89.

Konrad, J.-M. (1998). “Sand state from cone penetrometer tests: a framework considering grain crushing stress”. *Géotechnique*, 48(2), 201–215.

Lade, P. V. (2006). “Assessment of test data for selection of 3-D failure criterion for sand”. *Int. J. Numer. Anal. Met. Geomech.*, 30, 307–333.

Lee, J.-S. and Santamarina, J. C. (2005). “Bender elements: performance and signal interpretation”. *J. Geotech. Geoenviron. Eng.*, 10.1061/(ASCE)1090-0241(2005)131:9(1063), 1063–1070.

Li, X. S. and Dafalias, Y. F. (2000). “Dilatancy for cohesionless soils”. *Géotechnique*, 50(4), 449–460.

Li, X. S. and Wang, Y. (1998). “Linear representation of steady-state line for sand”. *J. Geotech. Geoenviron. Eng.*, 10.1061/(ASCE)1090-0241(1998)124:12(1215), 1215–1217.

Li, Y. and Bolton, M. (2014). “Energy conservation validates deformation mechanisms around model cantilever wall excavations in sand”. *Géotechnique*, 64(6), 419–430.

Ling, H. I. and Yang, S. T. (2006). “Unified sand model based on the critical state and generalized plasticity”. *J. Eng. Mech.*, 10.1061/(ASCE)0733-9399(2006)132:12(1380), 1380-1391.

Loukidis, D. and Salgado, R. (2009). “Modeling sand response using two-surface plasticity”. *Comput. Geotech.*, 36(1–2), 166–186.

Manzari, M. T. and Dafalias, Y. F. (1997). “A critical state two-surface plasticity model for sands”. *Géotechnique*, **47**, No. 2, 255–272.

Marques, A.S.P.S., Coelho, P.A.L.F., Haigh, S. and Madabhushi, G. (2014). “Centrifuge modeling of liquefaction effects on shallow foundations”. In *Seismic Evaluation and Rehabilitation of Structures*. *Geotech., Geol. Earthq. Eng.*, Springer, Switzerland, 26, 425–440.

Miura, S. and Toki, S. (1982). “A sample preparation method and its effect on static and cyclic deformation-strength properties of sand”. *Soils Found.*, 22(1), 61–77.

Mokni, M. and Desrues, J. (1999). “Strain localization measurements in undrained plane-strain biaxial tests on Hostun RF sand”. *Mech. Cohesive-Frictional Mat.*, 4, 419–441.

Murthy, T. G., Loukidis, D., Carraro, J. A. H., Prezzi, M. and Salgado, R. (2007). “Undrained monotonic response of clean and silty sands”. *Géotechnique*, 57(3), 273–288.

Papadimitriou, A. G. and Bouckovalas, G. D. (2002). “Plasticity model for sand under small and large cyclic strains: a multiaxial formulation”. *Soil Dyn. Earthq. Eng.*, 22(3), 191–204.

Pedro, A. (2013). *Geotechnical investigation of Ivens shaft in Lisbon*. Ph.D. dissertation, Imperial College London, London, U.K.

Riemer, M., Seed, R., Nicholson, P. and Jong, H.-L. (1990). “Steady state testing of loose sands: limiting minimum density”. *J. Geotech. Eng.*, 10.1061/(ASCE)0733-9410(1990)116:2(332), 332–337.

Roscoe, K. H. Schofield, A. N., and Wroth, C. P. (1958). “On the yielding of soils”. *Géotechnique*, 8(1), 22–53.

Saada, A., Puccini, P. and Bianchini, G. (1989). “Information package”. *Proc., Int. Workshop on Constitutive Equations for Granular Non-Cohesive Soils*, *Cleveland, 1987*, Balkema, Rotterdam, 81–88.

Sánchez-Salinero, I., Roesset, J. M. and Stokoe, K. H. (1986). “Analytical studies of body wave propagation and attenuation”. *Rep. No. GR86-15*, Univ. of Texas, Austin, Texas.

Schofield, A. and Wroth, P. (1968). *Critical state soil mechanics*. London: McGrawHill.

Vaid, Y. P., Chung, E. K. F. and Kuerbis, R. H. (1990). “Stress path and steady state”. *Can. Geotech. J.*, 27, 1-7.

Vaid, Y. P. and Sasitharan, S. (1992). “The strength and dilatancy of sand”. *Can. Geotech. J.*, 29, 522–526.

Verdugo, R. and Ishihara, K. (1996). “The steady state of sandy soils”. *Soils Found.*, 36(2), 81–91.

Viana da Fonseca, A., Ferreira, C. and Fahey, M. (2009). “A framework interpreting bender element tests, combining time-domain and frequency-domain methods”. *Geotech. Test. J.*, 32(2), 1–17.

Viggiani, G. and Atkinson, J. H. (1995). “Interpretation of bender element tests”. *Géotechnique*, 45(1), 149–154.

Wood, M., Belkheir, K. and Liu, D. (1994). “Strain softening and state parameter for sand modelling”. *Géotechnique*, 44(2), 335–339.

Yamamuro, J. and Lade, P. (1995). “Strain localization in extension tests on granular materials”. *J. Eng. Mech.*, 10.1061/(ASCE)0733-9399(1995)121:7(828), 828–836.

Yang, J. and Li X. S. (2004). “State-dependent strength of sands from the perspective of unified modeling”. *J. Geotech. Geoenviron. Eng.*, 10.1061/(ASCE)1090-0241(2004)130:2(186), 186–198.

Yoshimine, M., Ishihara, K., and Vargas, W. (1998). “Effects of principal stress direction and intermediate principal stress on undrained shear behavior of sand”. *Soils Found.*, 38(3), 179–188.

Zhou, Y. and Chen, Y. (2005). “Influence of seismic cyclic loading history on small strain shear modulus of saturated sands”. *Soil Dyn. Earthq. Eng.*, 25, 341–353.

Figure captions

Fig. 1. Particle size distribution curves of Hostun sand, Leighton Buzzard sand, Ottawa sand and Toyoura sand

Fig. 2. Schematic representation of the total stress paths followed in each type of triaxial test performed

Fig. 3. Selected first arrivals in time-domain (TD) and in frequency-domain (FD) at the selected stress levels, during the first loading of the ICDIC 0.794/25 test

Fig. 4. Values of the small-strain shear modulus estimated using the first arrival (time-domain) method for the ICDIC 0.794/25 and ICDIC 0.659/25 tests

Fig. 5. Small-strain shear modulus for Hostun sand

Fig. 6. Drained TC and TE tests with p'_0 = 80 kPa: (a) stress-strain and (b) volumetric strain as a function of the axial strain

Fig. 7. Undrained TC and TE tests with p'_0 = 80 kPa: (a) stress path, (b) stress-strain behaviour and (c) pore water pressure evolution with strain

Fig. 8. Prediction of the critical state line for Hostun sand

Fig. 9. Comparison of the proposed critical state line (CSL) with results presented in the literature

Fig. 10. Critical state strength of Hostun sand in compression and in extension

Fig. 11. Peak stress ratio as a function of the state parameter

Fig. 12. Stress ratio at phase transformation state as a function of the state parameter

Fig. 13. Stress-dilatancy relationship determined from drained TC tests

Table captions

Table 1. Physical properties of Hostun, Leighton Buzzard, Ottawa and Toyoura sands

Table 2. Summary of the initial conditions and results of the triaxial tests performed

Table 3. Characteristics of TC tests performed on Hostun sand at other institutions and used for comparing with the results obtained by the authors